NASA Technical Memorandum 106680

Modelling of Surfaces
Part I–Monatomic Metallic Surfaces Using Equivalent Crystal Theory

Guillermo Bozzolo
Analex Corporation
Brook Park, Ohio

John Ferrante
Lewis Research Center
Cleveland, Ohio

and

Agustín M. Rodríguez
Universidad Nacional de La Plata
La Plata, Argentina

July 1994

National Aeronautics and Space Administration

Modelling of Surfaces: I. Monatomic Metallic Surfaces using Equivalent Crystal Theory

Guillermo Bozzolo

Analex Corporation, 3001 Aerospace Parkway, Brook Park, OH 44142-1003

John Ferrante

National Aeronautics and Space Administration, Lewis Research Center, Cleveland, Ohio 44135

Agustín M. Rodríguez

Departamento de Física, Universidad Nacional de La Plata, C.C. 67, 1900 La Plata, Argentina

We present a detailed description of equivalent crystal theory focusing on its application to the study of surface structure. While the emphasis is in the structure of the algorithm and its computational aspects, we also present a comprehensive discussion on the calculation of surface energies of metallic systems with equivalent crystal theory and other approaches. Our results are compared to experiment and other semiempirical as well as first-principles calcualtions for a variety of fcc and bcc metals.

I. INTRODUCTION

Computational material science or the theory of materials has recently come of age. Calculation of properties of real materials at the atomic level such as grain boundary or dislocation energies or the dynamics thereof, which in the recent past have seemed intractable, now have some hope for realistic modelling. An even more startling assertion is that modelling of tribological phenomena is also now feasible. Tribology is a particularly difficult field for theoretical studies at the atomic level because of the different possible materials in contact under high loads, often with high degrees of disorder, but as Landman et al [1] have shown, a great deal of progress has been made in approaching problems of practical interest.

More generally, there has been tremendous progress in several areas in the field of material science, due largely to the advent of powerful theoretical techniques and a rapid growth in computational capabilities. As a result, the need for a 'theoretical laboratory' where materials can be modelled, and their properties studied, at will, has become a fundamental part of any industrial or scientific endeavour. In order to satisfy this need, however, it is of essential importance that the tools needed to implement such goal have to fullfill a number of conditions which not necessarily complement each other. On the one hand, physical accuracy is of paramount importance. In this sense, first-principles approaches are impressively successful, in that accurate agreement with experiment was obtained in several instances (band structure, transport and magnetic properties of solids, etc.). Properties of interest to the material scientist, however, are generally related to 'defects' in atomic structure which involve a partial loss of periodicity, and thus requiring calculations over a large number of atoms (dislocations, grain boundaries, interfaces between different materials, etc.). This poses an almost insurmountable obstacle, in that current technology prevents ab-initio calculations to have an acceptable level of computational efficiency to deal with problems dealing with a large number of atoms. For example, it is only recently became possible to predict which simple structure (fcc, bcc, hcp) for an elemental metal has the lowest energy [2].

On the other hand, in order to be able to perform realistic modelling within the constraints of the current available computer technology, the use of pair-potentials (two-body forces) offers an efficient alternative, but with a great deal of loss of physical accuracy, making them unreliable for predicting real material properties.

In the last decade, due to the obvious need to fill the gap between the two alternatives mentioned above, the use of semiempirical approaches emerged as the intermediate choice: based on sound physical concepts, they provide generally accurate results and with considerable computational efficiency over first-principles approaches. In general, semiempirical approaches tackle the many-body problem by determining a functional form for the cohesive energy based on some physical model, including some parameters determined by fitting to experimental properties. Once these constants are determined, the form is used to calculate the energy or dynamic behavior or other properties of interest, such as defect energies. While sometimes oversimplifying the problem, by the global treatment that is made of the electronic structure of the solid, the semiempirical approaches have proven to be extremelly effective in accomplishing its goals. A review of recent efforts dealing with calculation of properties of materials using semiempirical techniques shows that three methods dominate the research activity in this area: effective medium theory [3] (EMT), embedded atom method [4] (EAM) and equivalent crystal theory [5](ECT).

In this paper, we concentrate on equivalent crystal theory for the study of surface properties. More specifically, we present a detailed application of equivalent crystal theory to the calculation of surface energies and surface relaxations. Some previous studies [5,6] indicate that ECT provides, in general, a very good description of such surface properties, based on comparison with available experimental data. Most impressively, ECT was recently used to provide a simple description of the phenomenon of avalanche in adhesion [7]: at a certain separation , two approaching surfaces snap together, the critical distance for such event depending on the thickness of the metals in contact. This example demonstrates that calculational methods such as ECT enable examination of phenomena which are difficult to observe experimentally. Other recent application of ECT to surface phenomena include sur-

face reconstruction [8], modelling of atomic force microscopy [9], friction [10] and energetics of steps and kinks in metallic surfaces [11].

We organize this paper as follows: Section 2 provides a brief summary of ECT while Section 3 focuses on the application of the formalism to the calculation of surface energies and relaxations. Section 4 reviews the results obtained for a variety of metallic surfaces. We devote Section 5 to the discussion of advantages, limitations and general considerations for future applications of ECT for the computer modelling of materials and their properties.

II. EQUIVALENT CRYSTAL THEORY

Equivalent crystal theory [5] is based on an exact relationship between the total energy and atomic locations and applies to surfaces and defects in both simple and transition metals as well as in covalent solids. Lattice defects and surface energies are determined via perturbation theory on a fictitious, equivalent single crystal whose lattice constant is chosen to minimize the perturbation. Ferrante, Rose and Smith [12] found that the cohesive energy of metals and covalent solids as a function of varying the lattice parameter isotropically could be represented by a simple relationship,

$$E = E_C E^*(r^*) \tag{1}$$

where E_C is the cohesive energy and $E^*(r^*)$ is a universal shape for the curve, which can be well represented by the Rydberg function

$$E^*(r^*) = -(1 + r^*)e^{-r^*} \tag{2}$$

and

$$r^* = \frac{r - r_{WSE}}{l} \tag{3}$$

and where r is the Wigner-Seitz radius, r_{WSE} is the corresponding equilibrium value and l is given by

$$l = \left(\frac{E_C}{(d^2E/dr^2)_{r_{WSE}}} \right)^{1/2}, \tag{4}$$

which can also be written in terms of known experimental quantities as

$$l = \sqrt{\frac{E_C}{12\pi B r_{WSE}}}, \tag{5}$$

where B is the bulk modulus. The energy of the equivalent crystal, as a function of its lattice constant, can therefore be given by the universal binding energy relation (UBER) given by eq.(1). Fig. 1 displays total energy curves as a function of interatomic spacings for bimetallic adhesion and cohesion in metals as well as the UBER.

Let's consider a certain, arbitrary defect. Let ε be the total energy to form the defect or surface, then

$$\varepsilon = \sum_i \varepsilon_i \tag{6}$$

where ε_i is the contribution from an atom i close to the defect or surface. ECT is based on the concept that there exists, for each atom i, a certain perfect, equivalent crystal with its lattice parameter fixed at a value so that the energy of atom i in the equivalent crystal is also ε_i. This equivalent crystal differs from the actual ground-state crystal only in that its lattice constant may be different from the ground-state value. We compute ε_i via perturbation theory, where the perturbation arises from the difference in the ion core electronic potentials of the actual defect solid and those of the effective bulk single crystal.

For the sake of simplicity, the formal perturbation series is approximated by simple, analytic forms which contain a few parameters, which can be calculated from experimental results or first-principles calculations [5]. Our simplified perturbation series for ε_i is of the form

$$\varepsilon_i = E_C \left\{ F^* \left[a_1^*(i)\right] + \sum_j F^* \left[a_2^*(i,j)\right] + \sum_{j,k} \left[a_3^*(i,j,k)\right] + \sum_{p,q} F^* \left[a_4^*(i,p,q)\right] \right\} \tag{7}$$

where

$$F^* \left[a^*\right] = 1 - (1 + a^*)e^{-a^*} \tag{8}$$

$E_C F^*(a^*)$ uses the UBER described above to determine the change in energy of the equivalent crystal above the ground state value. In this expression, we distinguish four different contributions to the energy of atom i and thus, the existence of four different equivalent crystals which have to be determined for each atom i.

The first term, $F^* \left[a_1^*(i)\right]$, contributes when average neighbor distances are altered via defect or surface formation. It can be thought of as representing local atom density changes. In most cases, this 'volume' term is the leading contribution to ε_i and in the case of isotropic volume deformations, it gives ε_i to the accuracy of the UBER. The value of $a_1^*(i)$, the

lattice parameter of the first equivalent crystal associated with atom i, is chosen so that the perturbation (the difference in potentials between the solid containing the defect and its bulk, ground-state equivalent crystal) vanishes. Within the framework of ECT, this requirement translates into the following condition from which $a_1^*(i)$ is determined:

$$NR_1^p e^{-\alpha R_1} + MR_2^p e^{-(\alpha+\frac{1}{\lambda})R_2} - \sum_{defect} r_j^p e^{-[\alpha+S(r_j)]r_j} = 0 \tag{9}$$

where the sum over the defect crystal or surface is over all neighbors within second-neighbor (NNN) distance. r_j is the actual distance between atom i and a neighbor atom j, N and M are the number of nearest-neighbor (NN) and next-nearest-neighbors, respectively, of the equivalent crystal (12 and 6 for fcc, 8 and 6 for bcc) and p, α and λ are parameters known for each atomic species. Table 1 displays the values of these parameters for the fcc elements used in this work (see Ref. [5] for a complete list). $S(r_j)$ is a screening function and R_1 and R_2 are the NN and NNN distances in the equivalent crystal. The equivalent lattice parameter, a_1, is thus related to the scaled quantity a_1^* via

$$a_1^* = \left(\frac{R_1}{c} - r_{WSE}\right)/l, \tag{10}$$

where r_{WSE} is the equilibrium Wigner-Seitz radius, l is a scaling length and c is the ratio between the equilibrium lattice constant and r_{WSE}. Thus, the determination of the energy for an ion, in or near a defect, amounts to solving a simple transcendental equation for the equivalent lattice parameter.

The higher-order terms are relevant for the case of anisotropic deformations. The linear independence attributed to these four terms is consistent with the limit of small perturbations which we assume for the formulation of ECT. The second term, $F^*[a_2^*(i,j)]$, is a two-body term which accounts for the increase in energy when NN bonds are compressed below their equilibrium value. This effect is also modeled with an equivalent crystal, whose lattice parameter is obtained by solving a perturbation equation given by

$$NR_1^p e^{-\alpha R_1} - Nr_0^p e^{-\alpha r_0} + A_2 r_0^p \sum_j (R_j - r_0) e^{-\beta(R_j - r_0)} = 0, \tag{11}$$

where $\beta = 4\alpha$ for the metals used in this work, and R_1 is the NN distance of the equivalent crystal associated with the deviation of NN bond length R_j from r_0, and r_0 is the bulk NN distance at whatever pressure the solid is maintained (generally, r_0 is the ground-state, zero-pressure value). A_2 is a constant determined for each metal: for fcc metals A_2 is given by

$$a_e A_2/D = 1/6\sqrt{2} \tag{12}$$

and

$$a_e A_2/D = 1/4\sqrt{3} \tag{13}$$

for bcc metals. The quantity D is given by

$$D = Ne^{-\alpha r_0}(\alpha r_0 - p) \tag{14}$$

(see Table 1). The scaled equivalent lattice parameter is then

$$a_2^* = \left(\frac{R_1}{c} - r_{WSE}\right)/l. \tag{15}$$

The third term, $F^*[a_3^*(i,j,k)]$ accounts for the increase in energy that arises when bond angles deviate from their equilibrium values of the undistorted single crystal. This is a three-body term and the equivalent lattice parameter associated with this effect is obtained from the perturbation equation

$$NR_1^p e^{-\alpha R_1} - Nr_0^p e^{-\alpha r_0} + A_3 r_0^p e^{-\alpha(R_j+R_k-2r_0)} \sin(\theta_{jk} - \theta) = 0 \tag{16}$$

where A_3 is a constant listed in Table 1 and θ_{jk} is the angle between the NN distances R_j and R_k with the atom i at the center. θ is the equilibrium angle, 70.5° for bcc and 90° for fcc. This term contributes only when there is a bond-angle anisotropy ($\theta_{jk} \neq \theta$). The scaled lattice parameter is then

$$a_3^* = \left(\frac{R_1}{c} - r_{WSE}\right)/l. \tag{17}$$

The fourth term, $F^*[a_4^*(i,p,q)]$, describes face diagonal anisotropies (see Ref. [5] for a detailed description, for each lattice type, of the structural effect associated with this term). The perturbation equation reads

$$NR_1^p e^{-\alpha R_1} - Nr_0^p e^{-\alpha r_0} + A_4 r_0^p \frac{|d_p - d_q|}{d} e^{-\alpha(R_j+R_k+R_l+R_m-4r_0)} = 0 \tag{18}$$

where d is the face diagonal of the undistorted cube and A_4 is a constant adjusted to reproduce the experimental shear elastic constants (Table 1). Finally, $a_4^* = \left(\frac{R_1}{c} - r_{WSE}\right)/l$.

III. SURFACE ENERGY CALCULATION

A. Rigid surface

In this section, we illustrate the formalism described in the previous section, by providing a detailed application of ECT to the calculation of the surface energy of a metallic surface. Before we go through the details, we first make a few considerations of general interest regarding surface energy calculations and the simplifications introduced by certain assumptions.

Consider a rigid surface (i.e., no interlayer relaxation): all bond lengths and angles retain their bulk equilibrium values, thus $F^*(a_2^*) = F^*(a_3^*) = F^*(a_4^*) = 0$. The surface energy is therefore obtained by solving for the 'volume' term represented by $F^*(a_1^*)$ only. We note that for this case only, a single atom need be considered per plane since each site is equivalent and only a few planes should be included since convergence to bulk values occurs rapidly. If we consider a rigid displacement of the surface layer towards the bulk, as is the case in most metallic surfaces, the higher-order terms become finite: some bonds are compressed, contributing to $F^*(a_2^*)$, the bond angles near the surface are distorted as well as the difference between face diagonals in some cases, generating an increase of energy via $F^*(a_3^*)$ and $F^*(a_4^*)$. For the case studied in this work, these additional contributions to ε_i are generally small, representing only 1 % to 2 % of the total energy. However, while these anisotropy terms are small for metals when there is no reconstruction, they play an important role in the energetics of these defects where the differences in energy between the rigid and relaxed configurations are also small. In what follows, we will refer to this ECT formalism as ECT II [5].

As noted, the bond-angle and face-diagonal anisotropies are of very little interest for the calculation of metallic surface energies. For this case only, an earlier version of ECT [13], which we will refer to as ECT I, provides a simpler, although a bit less accurate framework for a surface energy calculation. The second term in eq.(7) is replaced by a

simple expression which allows for the direct calculation of the energy associated with bond-compression effects,

$$\varepsilon_2 = E_C \sum_{n=1}^{N_s} \sum_{m=1}^{M_n} \frac{\theta_{mn}}{L_{mn}} F^*(a^*_{mn}) \tag{19}$$

where N_s is the number of atoms in the solid, $\theta_{mn} = 1$ if $a^*_{mn} \leq 0$ and $\theta_{mn} = 0$ otherwise, M_n is the number of nearest-neighbors of atom n, L_{mn} is the number of nearest-neighbors of atom m or n, whichever number is smaller, and a^*_{mn} is given by

$$a^*_{mn} = \frac{R_{mn}/c_1 - r_{WSE}}{l}, \tag{20}$$

with

$$l = \sqrt{\frac{E_C}{12\pi B r_{WSE}}}, \tag{21}$$

B is the bulk modulus of the crystal, R_{mn} is the distance between atoms m and n, c_1 is the ratio of the equilibrium nearest-neighbor distance in the crystal to r_{WSE}, and r_{WSE} is the equilibrium Wigner-Seitz radius. In ECT I [13], the third and fourth term of the energy expansion (eq.(6)) are ignored. In what follows, we will list results as obtained with either one of the two versions of ECT. Those results obtained with the full energy expansion (ECT II) [5], will be analyzed in terms of the value of the parameter β which dictates the 'strength' of the bond compression term therefore playing an important role in the energetics of surface relaxation as it will be seen that this term is mainly responsible for avoiding the collapse of the top layers onto each other.

We now concentrate on the calculation of rigid surface energies with ECT. Each atom in each plane is equivalent to all other atoms in the plane, therefore it is only necessary to solve the ECT equations for a single atom in each plane and the only remaining question is how many planes are needed for convergence. Let's assume that the planes are labeled by an index j, $j = 1, ..., b$, where $j = 1$ indicates the surface plane and $j = b$ denotes a certain 'bulk' plane: a plane below which no surface effects are considered. For a single non-equivalent atom in plane j, we write the ECT equation

$$NR_1^p e^{-\alpha R_1} + MR_2^p e^{-(\alpha+\frac{1}{\lambda})R_2} = N_j r_1^p e^{-\alpha r_1} + M_j r_2^{-(\alpha+\frac{1}{\lambda})r_2} \tag{22}$$

where N and M are the number of nearest and next-nearest neighbors, respectively, in the perfect crystal ($N = 12, M = 6$ for fcc, $N = 8, M = 6$ for bcc, etc.). If there is no change in the interatomic distance between any pair of atoms, then all nearest neighbors and next-nearest neighbors in the defect crystal are separated by the same distance (r_1 and r_2, respectively), therefore, the last term in eq.(9) is greatly simplified as $r_j = r_1$ for the nearest neighbors and $r_j = r_2$ for the next-nearest neighbors. Moreover, the screening function adopts the values $S(r_1) = 0$ and $S(r_2) = 1/\lambda$, therefore avoiding further calculations. The values of N_j and M_j are easy to determine for each lattice type. Table 2 indicates some values for low index faces of fcc and bcc metals. We stress the point that all these simplifications are a consequece of assuming a rigid lattice, otherwise, each interatomic distance should be considered separately.

Finally, after eq.(22) is solved for all values of j, the corresponding solutions $R_1^{(j)}$ are used to evaluate the contribution to the surface energy σ_j:

$$\sigma_j = E_C F^*(a_j^*), \tag{23}$$

where

$$a_j^* = \frac{(R_1^{(j)}/c - r_{WSE})}{l} \tag{24}$$

and where F^* is given by eq.(8). The right hand side of eq.(22) is a measure of the defect (in this case, a surface). If the atom under consideration was a bulk atom in a perfect crystal, then $N_j = N$ and $M_j = M$, which states the obvious fact that the equivalent crystal coincides with the real crystal. Therefore, the quantity

$$Q_e = Nr_1^p e^{-\alpha r_1} + Mr_2^p e^{-(\alpha+\frac{1}{\lambda})r_2}, \tag{25}$$

where r_1 and r_2 represent the *equilibrium* nearest- and next-nearest-neighbor distances, respectively, can be considered as the reference magnitude for any defect. If we denote

with Q the r. h. s. of eq.(25), we then have three possibilities for any defect: a) if $Q = Q_e$, as noted above, the equivalent crystal for the atom in question is the equilibrium crystal itself, therefore, no additional calculation is necessary and that atom does not contribute any additional energy to the total energy of the defect crystal. It should be noted that $Q = Q_e$ does not mean that there is no defect present: it essentially means that the atom in question finds itself in a perturbed electron density that, in average, matches the one it would find in a perfect crystal. Therefore, we can say that the ground state of the equivalent crystal is 'degenerate', in the sense that many defects can be associated with such equivalent crystal. This is true, of course, for any other value of Q. b) if $Q > Q_e$, the defect represents a situation where the electron density is higher than in the perfect crystal. The corresponding equivalent crystal must have, as a consequence, a smaller lattice parameter than the perfect crystal. Conversely, c) if $Q < Q_e$ then the lattice parameter of the equivalent crystal is larger than the equilibrium value. Examples of the last two cases are, respectively, an interstitial atom and a vacancy.

As equivalent crystal theory is based on a perturbation expansion around the equilibrium crystal, one would expect the solutions of the ECT equation (eq.(9)) to display reasonably small deviations from $R_1 = r_0$, the equilibrium nearest neighbor separation. As a consequence, only those solutions of eq.(9) that are in the vicinity of r_0 are acceptable. Fig. 2 shows the graphical solution of Eq.(9): the curve indicates all the possible values of the l.h.s. of eq. (9), while the straight line indicates the measure of the defect, Q, while the dashed line corresponds to the equilibrium value Q_e. Two points are indicated in the horizontal axis: the equilibrium nearest-neighbor distance r_0, and the acceptable solution of Eq.(??). Solutions to the left of the peak of the curve should therefore be ignored.

In conclusion, the calculation of rigid surface energies is a straightforward procedure, which highlights the computational simplicity associated with ECT. This case is particularly simple because it only involves the calculation of the first term in Eq.(7) (no bonds are compressed and there are no bond-angle or face-diagonal anisotropies).

B. Relaxed surface

Letting the planes close to the surface relax, while introducing hardly any additional work in the calculation of the first term in eq.(7), it 'turns on' the other three contributions to the energy. As mentioned above, the last two terms are very small and we will, for the moment, neglect them. For the second term - the bond-compression term - we have, as discussed above, two options: the ECT I formalism [13], which introduces a simple counting procedure where no transcendental equation has to be solved: all that is needed is how many bonds between the atom in question and its nearest neighbors are compressed ($r < r_0$) and their length. The second option, ECT II [5], while using the same ingredients than ECT I, introduces a transcendental equation, eq.(11), in the same spirit as in eq.(9), where the anisotropy in bond length is considered as part of the perturbation.

For small compressions, there is no quantitative difference between the two alternatives. For larger compressions, the ECT II approach introduces an additional, adjustable parameter (β) which can be fitted to some property of the crystal that would provide a good description of such limiting situations. The basic qualitative difference between the two approaches is the fact that the ECT II approach provides a continuous contribution of the bond-compression energy as a function of bond length, whereas the ECT I version shows a discontinuity in the first derivative of the energy. While this is not a major drawback in modelling the defect, it could be a disadvantage when ECT is used in association with statistical techniques, where continuity in the derivatives of the energy could be a requirement.

Obviously, allowing the atoms in the surface region to relax, introduces the additional complexity of including more non-equivalent atoms to the calculation, located in deeper layers. As we will see in the following sections, this is unavoidable in the case of high-index faces, where several planes parallel to the surface plane have to be included even before a bulk-like environment is reached. Moreover, these cases require a careful treatment of relaxations perpendicular and parallel to the surface plane.

Many-atom effects, which are represented in ECT by the inclusion of the three-atom

bond-angle anisotropy and the four-atom face-diagonal distortion terms (see the third and fourth term in the r.h.s. of eq.(7)) are necessary but, in the case of surface energy calculations of metals, of very little relevance. As we will see below, they introduce a small correction usually of the order of 1 % of the leading term in eq.(7). That is not the case for semiconductors, where angular anisotropies are a significant contribution to the surface energy.

C. A simple example

For the sake of clarity, in what follows we provide a simple application to an fcc(100) metallic surface, where only the surface plane is allowed to relax. All atoms in a given plane are identical, therefore we only need to evaluate the contribution of one single non-equivalent atom per plane. Moreover, only three planes have to be considered in this calculation: atoms in the fourth plane and below find themselves in an equilibrium, bulk-like environment.

Fig. 3 shows a side view of such surface: the dots indicate atoms on the plane of the paper and the crosses indicate atoms one plane below or above. The top plane ($j = 1$) is slightly contracted, by a distance x toward the first plane below the surface ($j = 2$), but both the $j = 2$ and $j = 3$ planes, as well as any other plane below, are at equilibrium positions. The rigid interplanar spacing is $d = a_e/2$ (a_e is the equilibrium lattice parameter), therefore, the distance between $j = 1$ and $j = 2$ is $a_e/2 - x$. Following the labeling of Fig. 3 we write the ECT equations for the atoms A_1, B_1 and C_1, in terms of the distances r_{mn} between atoms m and n:

$$12R_1^p e^{-\alpha R_1} + 6R_2^p e^{-(\alpha+\frac{1}{\lambda})R_2} = 4r_{A_1A_2}^p e^{-\alpha r_{A_1A_2}} + 4r_{A_1B_1}^p e^{-\alpha r_{A_1B_1}} + 4r_{A_1A_3}^p e^{-(\alpha+\frac{1}{\lambda})r_{A_1A_3}} + r_{A_1C_1}^p e^{-(\alpha+\frac{1}{\lambda})r_{A_1C_1}} \quad (j=1) \tag{26}$$

$$12R_1^p e^{-\alpha R_1} + 6R_2^p e^{-(\alpha+\frac{1}{\lambda})R_2} = 8r_{B_1B_2}^p e^{-\alpha r_{B_1B_2}} + 4r_{B_1A_1}^p e^{-\alpha r_{B_1A_1}} + 5r_{B_1B_3}^p e^{-(\alpha+\frac{1}{\lambda})r_{B_1B_3}} \quad (j=2) \tag{27}$$

$$12R_1^p e^{-\alpha R_1} + 6R_2^p e^{-(\alpha+\frac{1}{\lambda})R_2} =$$

$$12r_{C_1C_2}^p e^{-\alpha r_{C_1C_2}} + 5r_{C_1C_3}^p e^{-(\alpha+\frac{1}{\lambda})r_{C_1C_3}} + r_{C_1A_1}^p e^{-(\alpha+\frac{1}{\lambda})r_{C_1A_1}} \quad (j=3) \qquad (28)$$

where

$$r_{A_1A_2} = r_{B_1B_2} = r_{C_1C_2} = r_0 = \frac{\sqrt{2}}{2}a_e \qquad (29)$$

$$r_{A_1B_1} = r_{B_1A_1} = r_x = \sqrt{\left(\frac{a_e}{2}\right)^2 + x^2} \qquad (30)$$

$$r_{A_1A_3} = r_{B_1B_3} = r_{C_1C_3} = s_0 = a_e \qquad (31)$$

and

$$r_{A_1C_1} = r_{C_1A_1} = s_x = a_e - x. \qquad (32)$$

Eqs.(26)-(28) are then solved, for each value of x, for the lattice parameter $a_E^{(j)}$ of the corresponding equivalent crystal:

$$a_E^{(j)}(x) = R_2^{(j)} = \sqrt{2}R_1^{(j)} \qquad j = 1,2,3. \qquad (33)$$

Finally, the 'volume' contribution to the surface energy is

$$\sigma_1 = \sum_{j=1}^{3} \sigma_1^{(j)} = E_C \sum_{j=1}^{3} F^*(a_{1,j}^*(x)) \qquad (34)$$

where

$$a_{1,j}^* = \frac{1}{l}(\frac{R_1^{(j)}}{c} - r_{WSE}), \qquad (35)$$

and F^* is given by eq.(8).

We now compute the bond length anisotropy contribution to the surface energy. Within the ECT I framework, the contribution is given by eq.(19):

$$\sigma_2^{ECTI} = E_C(\frac{1}{8}F^*(a_{A_1B_1}^*) + \frac{1}{8}F^*(a_{B_1A_1}^*)) \qquad (36)$$

where

$$a^*_{A_1B_1} = a^*_{B_1A_1} = \frac{r_x/c_1 - r_{WSE}}{l}. \tag{37}$$

as long as $x > 0$. If $x < 0$ then $\sigma_2^{ECTI} = 0$.

In order to compute the bond-compression contribution within the ECT II framework, we need to solve the following transcendental equation in order to find the equivalent crystals (for atoms A_1 and B_1) associated with this defect:

$$12R_1^p e^{-\alpha R_1} - 12r_0^p e^{-\alpha r_0} + 4A_2 r_0^p (r_x - r_0) e^{-\beta(r_x - r_0)} = 0 \quad (atom\ A_1) \tag{38}$$

The equation for atom B_1, for this particular example, is identical to eq.(38) (reflecting the identity $a^*_{B_1A_1} = a^*_{A_1B_1}$ for the ECT I case). Eq.(38) is then solved with respect to R_1 and the energy contribution is then

$$\sigma_2^{ECTII} = E_C F^*(a_2^*(x)) \tag{39}$$

where a_2^* is given by eq.(15).

The third term in eq.(7) deals with bond-angle anisotropies. Contributions to σ_3 come from atoms for which the angle between its nearest neighbors departs from its equilibrium value θ_0 ($\theta_0 = 90°$ for fcc). Following the convention described in ref. [5] that says that if an atom is missing one or more nearest-neighbors, then $F^*(a_3^*(i,j,k)) = 0$ for that atom, then the atoms in the top layer do not contribute to σ_3. The only contribution then arises from the atoms in the first layer below the surface ($j = 2$), for which we solve the transcendental equation (see eq.(16))

$$12R_1^p e^{-\alpha R_1} - 12r_0^p e^{-\alpha r_0} + A_3 r_0^p e^{-\alpha(r_x - r_0)} \sin|\theta - \theta_0| = 0 \tag{40}$$

where

$$\theta = \cos^{-1}\left\{\frac{r_x^2 + r_0^2 - s_x^2}{2r_x r_0}\right\}. \tag{41}$$

Eq.(40) is solved with respect to R_1 and the bond-angle contribution is then

$$\sigma_3^{ECTII} = 4E_C F^*(a_3^*(x)), \tag{42}$$

where a_3^* is given by eq.(17).

For the particular case of the fcc (100) face, the fourth term vanishes, as the diagonals associated with each atom in the layer $j = 2$ do not change relative to each other, although the length of each diagonal is different from the equilibrium value.

Summarizing, the surface energy of an fcc(100) face, where only the top layer is allowed to relax is given by

$$\sigma^{ECTI} = E_C\{\sum_{j=1}^{3} F^*(a_{1,j}^*(x)) + \frac{1}{4}F^*(a_{A_1B_1}^*)\} \tag{43}$$

where $a_{1,j}^*(x)$ and $a_{A_1B_1}^*$ are given by eqs.(35) and (37), respectively. Within the ECT II formalism, σ is given by

$$\sigma^{ECTII} = E_C\{\sum_{j=1}^{3} F^*(a_{1,j}^*(x)) + F^*(a_2^*(x)) + 4F^*(a_3^*(x))\} \tag{44}$$

where $a_2^*(x)$ and $a_3^*(x)$ are given by eqs.(15) and (17), respectively.

IV. RESULTS

ECT, in any of its two versions, has been applied with a great deal of success to several problems involving surface phenomena [5–10]. In the case of surface energies, ECT is particularly successful as it gives a very good approximation to the currently accepted experimental and first-principles values, therefore making it a good candidate for predicting such quantity in other cases. We have carried out an extensive calculation of surface energies of fully relaxed (but unreconstructed) surfaces of several fcc and bcc metals, and for a variety of choices for the Miller indices, ranging from (111) to (771) [6]. Although some of these surfaces are known to reconstruct, we did not look for this effect in our calculations with the sole purpose of generating a large data set of surface energy values from which patterns can be extracted, by studying the dependence of surface energy on several variables (Miller indeces, cohesive energy, roughness [14], borocity [15], lattice structure, etc.).

In the previous section, we repeatedly mentioned the fact that the many-body anisotropies (bond-angle, face-diagonal) that appear in the ECT II formalism are not of great relevance for the calculation of surface energies. This point is proven by the results displayed in Table 3 where we show some results for low- and high-index faces, both rigid and fully relaxed, for the surface energy and the different contributions arising from the ECT II expansion (eq.(7)). Table 4 proves another point made in the previous section: in general, both ECT I and ECT II give results of comparable quality in the case of surface energies.

Tables 5 and 6 display an extensive set of results for fcc and bcc metals, where we compare with several experimental estimates as well as the surface energies obtained by other approaches. First, we examine the quality of our results by comparison with first-principles calculations. First-principles values do not suffer from the ambiguities in surface geometry and cleanliness as the difficult to obtain experimental values. The surface energy for polycrystalline solids is usually assumed to be close to that of the most dense (less rough) surface, therefore we discuss results for the densest packed fcc (111) planes. We extract our

values from Tables 5 and 6, for direct comparison with other methods for which we could find surface energies , where the first number will be the ECT II value, (), the second EAM [4,19], [], the third Finnis-Sinclair [16], [[]], and the last first-principles [17], {} (all values are in ergs/cm^2): Cu (1758), [1170,1184], {2100}; Ag (1221), [620,655], [[620]], {1221}; Pd (1696), [1220,1050], {1640}. We can see that in all cases ECT II agrees extremelly well with first-principles results, whereas Finnis-Sinclair and EAM results can be as much as 50 % low.

The next comparison made is with the planar anisotropy of the surface energy as obtained by different approaches. There are arguments [17,18] for expecting the variation in the surface energy from plane to plane to be smaller than expected from variations in surface roughness. For example, as mentioned earlier, electron smoothing in order to reduce the kinetic energy could reduce the variation in surface energy expected from roughness variations. For this discussion, we reproduce results presented by Methfessel et al [17] (table 7) with additional analysis, updated values for ECT from the present paper, and more recent EAM results [19]. First we note that when we examine the anisotropy ratios $\gamma_{110-111} = \sigma_{110}/\sigma_{111}$ and $\gamma_{100-111} = \sigma_{100}/\sigma_{111}$, where σ_{hkl} is the surface energy of the face (hkl), as well as $\gamma_{100-110} = \sigma_{100}/\sigma_{110}$, Methfessel et al's assertion that the other semi-empirical methods, EAM and Finnis-Sinclair, show a smaller surface anisotropy than ECT is not substantiated. The surface anisotropies predicted by the three methods are actually quite close and all three predict a small variation between the values of $\gamma_{100-110}$.

A simple modification of ECT II can bring the surface anisotropy much closer to the Methfessel et al values [17]. As we stated earlier, ECT introduces a screening function for next and higher order neighbors [5] based on the bulk screening length. The functional form for this screening is assumed to be an exponential which although reasonable, is ad hoc. Assuming no screening (Table 8) for both Pd and Ag, the surface anisotropy variation can be brought much more in line with the values reported in ref. [17], without affecting the outstanding agreement for the surface energies for the (111) surfaces. We note that such an assignment of screening length is directly comparable to that used in EAM. We

further note that there is not at present a consistent comparison between first-principles and semiempirical methods. Limiting our example to ECT, the primary input parameters for the method are the experimental values for the cohesive energy, the zero-pressure bulk modulus, the equilibrium lattice parameter and the vacancy formation energy. In order to make a consistent comparison it would be necessary to use input values from the first-principles calculations for determination of the fitting parameters in each method.

Next we address the bcc structure metals. Our values for the ratios $\gamma_{100-110} = \sigma_{100}/\sigma_{110}$ and $\gamma_{111-110} = \sigma_{111}/\sigma_{110}$ for W and Fe are, respectively, $\gamma_{100-110} = 1.78, 1.97$ and $\gamma_{111-110} = 1.32, 1.40$. The values of Methfessel et al [17] and Finnis-Sinclair [16] for $\gamma_{100-110}$ are respectively, 1.21 and 1.17 for Nb and 1.13 and 1.15 for Mo. Here, the assertion in ref. [17] is more accurate, however we note that for the only first-principles comparisons that we have found for a bcc system, that is, W, Fe (100), the ECT value of 5808 ergs/cm^2 as compared to 5100 ergs/cm^2 for W (100) [20] (an overestimate of 14 %) and 3353 ergs/cm^2 as compared to 3100 ergs/cm^2 for Fe (100) [21] (an overestimate of 8 %) are in quite good agreement. Although the surface anisotropy seems high in this case, there is as yet no complete test of the bcc systems which warrant a definite conclusion. As mentioned above, we have shown that a simple modification of ECT can be made which corrects for the seeming discrepancy in surface anisotropy while maintaining the simplicity of the method and the highly accurate predictions for the surface energies of the densest packed planes.

Simple bond-cutting arguments have been used to explain the face dependence of the surface energy, which could be thought of as the energy cost for cutting the bonds to one nearest-neighbor times the number of removed NN atoms in the process of surface formation. ECT provides a simple qualitative and quantitative description of this process: if we consider a rigid surface (so that second-order effects due to anisotropies are not included), one would reasonably expect the atoms in the top layers to be mostly affected by the creation of the surface. For example, for fcc (100) planes, the contribution of an atom in the surface plane accounts for most of the surface energy, while atoms in the second layer contribute less than 1 %. The ECT equation for determining the lattice parameter of the equivalent crystal

associated with an atom on the surface is (see eq.(22))

$$NR_1^p e^{-\alpha R_1} + MR_2^p e^{-(\alpha+\frac{1}{\lambda})R_2} = N_1 r_1^p e^{-\alpha r_1} + M_1 r_2^p e^{-(\alpha+\frac{1}{\lambda})r_2}, \tag{45}$$

where N_1 and M_1 represent the number of NN and NNN of the atom on the surface (thus, $N - N_1$ and $M - M_1$ are the number of NN and NNN bonds broken in the process of creating the surface). R_1 and R_2 are the NN and NNN distances in the equivalent crystal of lattice parameter a_{EQ}. This is a transcendental equation for a_{EQ} and although it cannot be solved analytically, it can be shown that a simple linear approximation gives a result for a_{EQ} which is only 10 % off the exact value. This approximation entails a linear dependence on the number of broken bonds, $N - N_1$ and $M - M_1$. The dependence of the surface energy on these quantities is given by the Rydberg function, thus establishing a relationship between surface energy, cohesive energy and the number of NN and NNN broken bonds,

$$\sigma_{surf} = E_C\{1 - (1 + a^*)e^{-a^*}\}. \tag{46}$$

where a^* is the scaled lattice paramater of the equivalent crystal:

$$a^* = q\frac{(a_{EQ} - a_e)}{l}. \tag{47}$$

The previous analysis provides a simple explanation for the differences in surface energy between different planes. Nevertheless, the surface energies obtained with ECT compare very well with experiment in all cases, as shown in Tables 5 and 6 where the ECT predictions, as well as other theoretical and experimental figures are displayed for fcc (Table 5) and bcc (Table 6) metals.

We once again note that the surfaces energies displayed are for relaxed but unreconstructed surfaces. This is obviously unrealistic for high-index faces, or even cases like Au (100), but it provides a rough idea of the dependence of the surface energy on the roughness of the surface. A comparison of the results in Table 5 (obtained with ECT II allowing only for planar relaxations in a direction perpendicular to the surface plane) and the surface energies quoted in Table 4 (which also include atomic relaxations parallel to the surface

plane) shows that adding this degree of freedom in the calculation, while introducing a significant change in terms of the number of variables with respect to which the energy has to be minized, introduces little or no change in the values of the surface energy.

V. CONCLUSIONS

Equivalent crystal theory, like other semiempirical techniques, is supposed to narrow the gap between formal first-principles calculations and empirical approaches. To achieve this goal, ECT provides a simple operational procedure with minimal computational complexity. At the same time, it has a strong foundation on perturbation theory. In the case of surface phenomena, ECT is an excellent tool for describing the different aspects of surface structure and, as we intended to show in this work, allows for simple visualization of the relevant features.

It is an encouraging fact that, in spite of the reasonable success obtained in the applications studied since the inception of this method, it is amenable to extensions in a straightforward fashion: a quick analysis of the perturbation series expansion provides clear indication of how the method can be perfected to deal with more complex situations. This flexibility is a necessary condition for any method that attempts to describe, in one single scheme, all possible systems.

ACKNOWLEDGMENTS

Fruitful discussions with Dr. N. Bozzolo are gratefully acknowledged. This work was partially supported by the Engineering Directorate, NASA Lewis Research Center.

REFERENCES

[1] U. Landman, W. D. Luedtke and E. M. Ringer in Fundamentals of Friction, Eds. I. L. Singer and H. M. Pollock, NATO ASI Series, Kluwer Academic Publishers, The Netherlands, 1992.

[2] H. L. Skriver, Phys. Rev. Lett. **49**, 1968 (1982); M. T. Yin and M. L. Cohen, Phys. Rev. B **26**, (1982).

[3] J. K. Norskov, Phys. Rev. B **20**, 446 (1979).

[4] S. M. Foiles, M. I. Baskes and M. S. Daw, Phys. Rev. B **33**, 7893 (1986).

[5] J. R. Smith, T. Perry, A. Banerjea, J. Ferrante and G. Bozzolo, Phys. Rev. B **44**, 6444 (1991).

[6] A. M. Rodríguez, G. Bozzolo and J. Ferrante, Surf. Sci. **289**, 100 (1993) and refrences therein.

[7] J. R. Smith, G. Bozzolo, A. Banerjea and J. Ferrante, Phys. Rev. Lett. **63**, 1269 (1989).

[8] B. Good and A. Banerjea, Mat. Res. Soc. Symp. Proc. **278**, 211 (1992).

[9] A. Banerjea, J. Ferrante and J. R. Smith, J. Phys.: Condens. Matter **2**, 8841 (1990).

[10] G. Bozzolo, J. Ferrante and J. R. Smith, Scripta Met. Mater. **25**, 1927 (1991).

[11] S. Khare and T. Einstein (private communication)

[12] J. H. Rose, J. R. Smith and J. Ferrante, Phys. Rev. B **28**, 1835 (1983); J. H. Rose, J. R. Smith, F. Guinea and J. Ferrante, Phys. Rev. B **29**, 2963 (1984).

[13] J. R. Smith and A. Banerjea, Phys. Rev. Lett. bf 59, 2451 (1987); *ibid.*, Phys. Rev. B **37**, 10411 (1988).

[14] J. Sokolov, F. Jona and P. M. Marcus, Sol. State Comm. **49**, 307 (1984).

[15] G. Bozzolo, A. M. Rodríguez and J. Ferrante, Surf. Sci. (in press).

[16] M. W. Finnis and J. E. Sinclair, Philos. Mag. A **50**, 45 (1984).

[17] M. Methfessel, D. Hennig and M. Scheffler, Phys. Rev. B **46**, 4816 (1992).

[18] J. P. Perdew, Y. Wang and E. Engel, Phys. Rev. Lett. **66**, 508 (1991).

[19] T. Ning, Q. Yu and Y. Ye, Surf. Sci. **206**, L857 (1988); T. Ning and Y. Ye (private communication).

[20] C. L. Fu, S. Ohnishi, H. F. Jansen and A. J. Freeman, Phys. Rev. B **31**, 1168 (1985).

[21] J. G. Gay, J. R. Smith, R. Richter, F. J. Arlinghaus and R. H. Wagoner, J. Vac. Sci. Technol. A **2**, 931 (1984); J. R. Smith, J. Ferrante, P. Vinet, J. G. Gay, R. Richter and J. H. Rose, in : Chemistry and Physics of Fracture, Eds. R. H. Jones and R. M. Latanision (Nijhoff, Hingham, MA, 1987).

[22] K. -M. Ho and K. P. Bohnen, Phys. Rev. B **32**, 3446 (1985).

[23] J. A. Appelbaum and D. R. Hamann, Sol. State Comm. **27**, 881 (1978).

[24] W. R. Tyson, J. Appl. Phys. **47**, 459 (1976), and references therein.

[25] W. R. Tyson and W. A. Miller, Surf. Sci. **62**, 267 (1977).

[26] D. Wolf, Surf. Sci. **226**, 389 (1990).

[27] S. P. Chen and A. F. Voter, Surf. Sci. **244**, L107 (1991).

[28] M. Weinert, R. E. Watson, J. W. Davenport and G. W. Fernando, Phys. Rev. B **39**, 12585 (1989).

[29] G. J. Ackland and M. W. Finnis, Philos. Mag. A**54**, 301 (1986); G. Ackland, G. Tichy, V. Vitek and M. W. Finnis, *ibid.* A**56**, 735 (1987).

[30] S. P. Chen, Surf. Sci. **274**, L619 (1992).

[31] L. E. Murr, in Interfacial Phenomena in Metals and Alloys, Addison-Wesley, Reading,

MA, 1975.

[32] W. R. Tyson, R. A. Ayres and D. F. Stein, Acta Met. **21**, 621 (1973).

[33] J. J. Gilman, in Fracture, edited by B. L. Averbach, D. K. Felbeck, G. T. Hahn and D. A. Thomas, John Wiley, NY, 1959.

[34] A. G. Gvozdev and L. I. Gvozdeva, Fiz. Met. Metalloved **31**, 640 (1971).

[35] M. H. Richman, Trans. ASM, **60**, 719 (1967).

[36] E. N. Hodkin, M. G. Nicholas and D. M. Poole, J. Less-Common Met. **20**, 93 (1970).

[37] G. Treglia, M. C. Desjonquere and D. Spanjaard, J. Phys. C: Condens. Matter **16**, 2407 (1983).

[38] C. T. Chan and S. G. Louie, Phys. Rev. B **33**, 2861 (1986).

Element	p	l	α	λ	$10^{-2}A_3/D$	$10^{-1}A_4/D$	$10^{-4}D$	ΔE	a_e
Al	4	0.336	2.105	0.944	7.822	2.104	591.4	3.34	4.05
Cu	6	0.272	2.935	0.765	5.784	2.530	99.74	3.50	3.615
Ag	8	0.269	3.337	0.756	5.390	2.285	12.90	2.96	4.086
Au	10	0.236	4.339	0.663	4.047	1.673	1.127	3.78	4.078
Ni	6	0.270	3.015	0.759	7.382	2.793	100.1	4.435	3.524
Pd	8	0.237	3.612	0.666	5.242	2.012	11.25	3.94	3.89
Pt	10	0.237	4.535	0.666	5.789	1.727	1.071	5.85	3.92
Fe	6	0.277	3.124	0.770	9.183	1.887	60.62	4.29	2.86
W	10	0.274	4.232	0.770	12.03	1.497	1.179	8.66	3.16

Table 1: Computed constants and experimental input for ECT II. The constant p is $2n-2$, where n is the atomic principal quantum number, l (in Å) is a screening parameter (see text). The constants A_3 and A_4 are dimensionless. E_C (in eV) is the cohesive energy and a_e (in Å) is the equilibrium lattice constant.

j	(hk$l$)	fcc		bcc	
		N_j	M_j	N_j	M_j
1	(100)	8	5	4	5
	(110)	7	4	6	4
	(111)	9	3	4	3
2	(100)	12	5	8	5
	(110)	11	4	8	6
	(111)	12	6	7	3
3	(100)	12	6	8	6
	(110)	12	6	8	6
	(111)	12	6	7	6

Table2: Number of nearest-neighbors (N_j) and next-nearest-neighbors (M_j) of an atom in plane j ($j = 1$ is the surface plane) for (hkl) fcc and bcc surfaces.

	hkl	Rigid	Relaxed	σ_1	σ_2	σ_3	σ_4
	111	1813.90	1757.63	1735.83	20.48	0.00	1.32
	100	2362.26	2301.70	2276.59	22.61	2.51	0.00
	110	2443.38	2365.87	2335.63	28.32	0.00	1.92
Cu	311	2432.55	2363.21	2335.13	25.72	1.06	1.30
	331	2306.33	2237.46	2210.38	24.88	0.04	2.16
	210	2617.94	2543.69	2514.30	27.31	0.32	1.75
	211	2288.15	2227.98	2203.65	22.03	0.57	1.72
	310	2598.22	2528.68	2500.59	26.06	0.90	1.13
	111	1752.92	1695.55	1673.79	20.98	0.00	0.78
	100	2303.30	2240.53	2215.23	23.26	2.04	0.00
	110	2382.47	2303.44	2273.40	28.87	0.00	1.17
Pd	311	2368.39	2297.26	2269.23	26.29	0.93	0.81
	331	2242.51	2172.17	2145.44	25.34	0.03	1.35
	210	2553.10	2477.53	2448.79	27.41	0.26	1.07
	211	2223.16	2157.22	2131.50	24.02	0.58	1.12
	310	2533.69	2462.54	2434.30	26.79	0.70	0.75
	110	1778.77	1703.92	1671.38	28.43	2.88	1.21
	100	3447.37	3353.12	3307.87	39.89	5.36	0.00
	211	2228.52	2131.37	2091.82	36.28	0.32	2.95
Fe	310	2978.04	2866.88	2798.64	57.92	8.10	2.22
	111	2477.70	2390.38	2355.99	31.82	0.01	2.56
	210	2668.29	2583.46	2540.82	36.62	4.31	1.71
	311	2685.95	2578.01	2529.75	43.93	2.16	2.17
	331	2139.92	2050.28	2005.81	37.39	3.72	3.35

Table 3:Rigid and relaxed surface energies (in erg/cm^2) for Cu, Pd, and Fe surfaces. σ_j ($j = 1, ..., 4$) denotes the contribution to the surface energy from the j term in the ECT expansion.

Surface	Rigid	ECT I	ECT II
$\sigma^{Al}_{(210)}$	1493	1424	1404
$\sigma^{Ni}_{(210)}$	3407	3330	3306
$\sigma^{Cu}_{(210)}$	2618	2559	2540

Table 4: Surface energies (in erg/cm^2) of the rigid and relaxed (210) surfaces of Al, Ni and Cu computed with ECT I and II.

Face	Al	Cu	Ag	Au	Ni	Pd	Pt
Exp.	1140[25] 1180[25] 1200[24]	1780[25] 1770[25] 1790[24]	1240[25] 1320[25] 1340[24]	1500[25] 1540[25] 1560[24]	2380[25] 2240[25] 2270[24]	2000[25]	2490[25] 2590[24]
(111)	856[6]	1758[6] 1170[4] 1184[19] 2100[23] 839[26]	1221[6] 1210[17] 620[4] 655[19] 620[29]	1132[6] 790[4] 741[19] 767[26]	2275[6] 1450[4] 1284[19]	1696[6] 1640[17] 1220[4] 1050[19]	1716[6] 1440[4] 1191[19]
(100)	1209[6]	2302[6] 1280[4] 1367[19] 2300[21] 892[26]	1583[6] 1210[17] 705[4] 795[19] 1650[21] 1300[28] 750[29]	1547[6] 918[4] 906[19] 897[26]	2988[6] 1580[4] 1535[19] 3050[21]	2241[6] 1860[17] 1370[4] 1249[19] 2300[28]	2368[6] 1650[4] 1476[19]
(110)	1286[6] 1100 [16] 959[27]	2366[6] 1400[4] 1514[19] 957[26] 1471[27]	1619[6] 1260[17] 770[4] 887[19] 967[27] 1400[28] 810[29]	1622[6] 980[4] 999[19] 957[26] 969[27]	3076[6] 1730[4] 1733[19] 1977[27]	2303[6] 1970[17] 1490[4] 1366[19] 1708[27] 2500[28]	2496[6] 1750[4] 1652[19] 1681[27]
(311)	1263[6]	2363[6] 1494[19] 961[26]	1622[6] 868[19]	1601[6] 980[19] 944[26]	3068[6] 1702[19]	2297[6] 1345[19]	2458[6] 1618[19]
(331)	1180[6]	2237[6] 1460[19]	1538[6] 841[19]	1506[6] 954[19]	2905[6] 1654[19]	2172[6] 1312[19]	2307[6] 1573[19]
(210)	1407[6] 999[27]	2544[6] 1620[19] 1544[27]	1738[6] 963[19] 1014[27]	1758[6] 1090[19] 1028[27]	3310[6] 1878[19] 2082[27]	2478[6] 1465[19] 1890[27]	2714[6] 1814[19] 1777[27]
(211)	1165[6]	2228[6] 1433[19]	1533[6] 823[19]	1490[6] 936[19]	2892[6] 1619[19]	2157[6] 1291[19]	2281[6] 1541[19]
(310)	1379[6] 977[27]	2529[6] 1510[27]	1731[6] 992[27]	1734[6] 999[27]	3288[6] 2029[27]	2463[6] 1851[27]	2671[6] 1734[27]

Table 5: Experimental (Exp.) and theoretical surface energies for fcc metals.

Face	Fe	W
Exp.	2410[25]	2800[31]
	2360[25]	2830[36]
	2370[24]	3250[25]
		2990[25]
		3070[24]
(110)	1704[6]	3258[6]
	1210[32]	2683[30]
	1710[33]	3480[32]
	1720[34]	3320[33]
		7740[34]
		3240[35]
(100)	3353[6]	5808[6]
	3100[21]	5100 [20]
	1310[32]	4950[38]
	1440[33]	3252[30]
	1950[34]	3720[32]
	1693[16]	4680[33]
		7770[34]
		3590[35]
		3047[37]
		2926[16]
(211)	2131[6]	3932[6]
		3224[30]
(111)	2390[6]	4290[6]
	5340[33]	3510[30]
	2630[34]	8130[33]
		8430[34]
		2350[35]

Table6 : Experimental (Exp.) and theoretical surface energies for bcc metals.

		DFT Ref. 17	FLAPW Ref. 28	FS Ref. 29	EAM Ref. 4	EAM Ref. 19	ECT
Pd	σ_{111}	1.64			1.22	1.05	1.69
	σ_{100}	1.86	2.3		1.37	1.25	2.24
	σ_{110}	1.97	2.5		1.49	1.37	2.30
Pd	$\gamma_{100-111}$	1.13			1.12	1.19	1.32
	$\gamma_{110-111}$	1.20			1.22	1.30	1.36
	$\gamma_{100-110}$	0.94	0.92		0.92	0.91	0.97
Ag	σ_{111}	1.21		0.62	0.62	0.65	1.22
	σ_{100}	1.21	1.3	0.76	0.71	0.79	1.58
	σ_{110}	1.26	1.4	0.81	0.77	0.89	1.62
Ag	$\gamma_{100-111}$	1.00		1.22	1.14	1.21	1.29
	$\gamma_{110-111}$	1.04		1.31	1.24	1.37	1.33
	$\gamma_{100-110}$	0.96	0.93	0.94	0.92	0.89	0.97

Table 7: Comparison of ECT surface energies (in erg/cm^2) for Pd and Ag with results of full-potential LAPW calculations (ref. 17), Finnis-Sinclair (ref. 29) and EAM (refs. 4, 19) semiempirical results. σ_{hkl} denotes the surface energy of the (hkl) surface and $\gamma_{hkl-hkl'}$ denotes the ratio between σ_{hkl} and $\sigma_{hkl'}$.

		$\sigma^{ECT}_{scr.}$	$\sigma^{ECT}_{no-scr.}$	Ref. 17
Ag	(100)	1613	1220	1210
	(110)	1660	1440	1260
	(111)	1250	1200	1210
Pd	(100)	2300	1800	1860
	(110)	2380	2090	1970
	(111)	1750	1700	1640

Table8: Comparison of the surface energies (in erg/cm^2) of the low-index faces of Ag and Pd obtained with ECT and first-principles calculations (ref. 17).

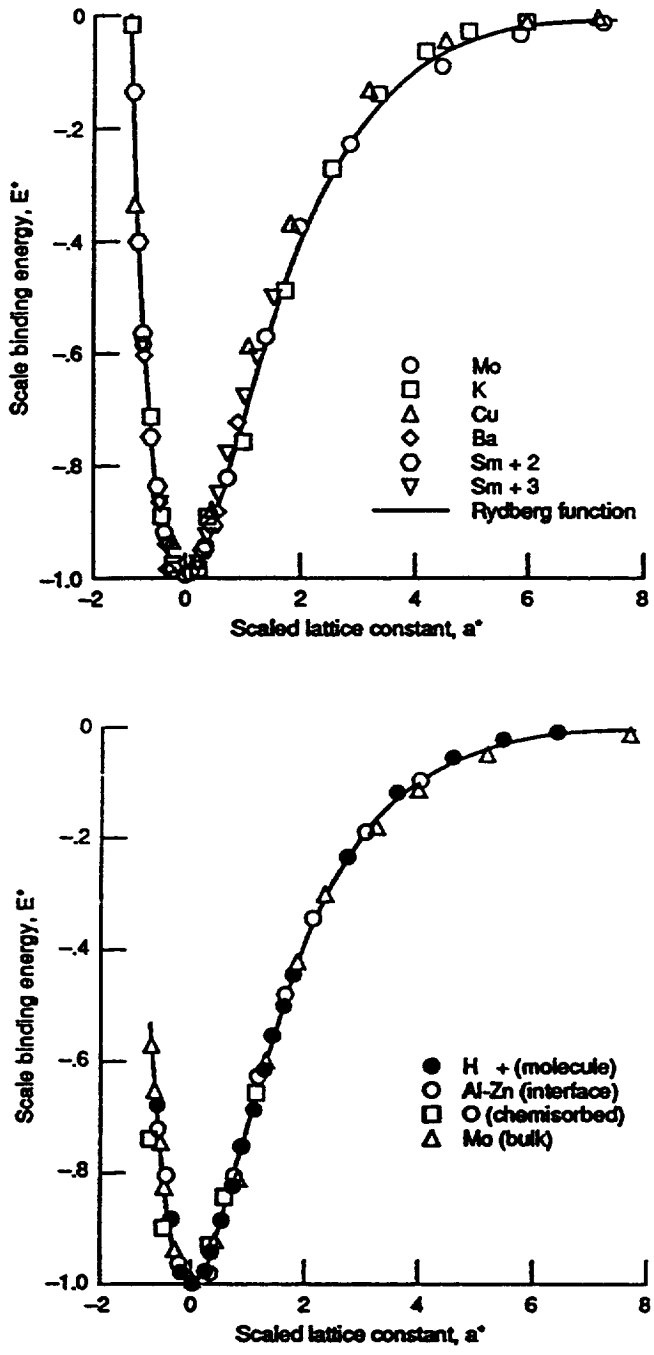

Fig. 1: (a) Scaled binding energy per atom of a crystal as a function of interatomic separation for representative solids. (b) Scaled binding energy versus scaled separation for representative cases of cohesion, bimetallic adhesion, chemisorption and diatomic molecule.

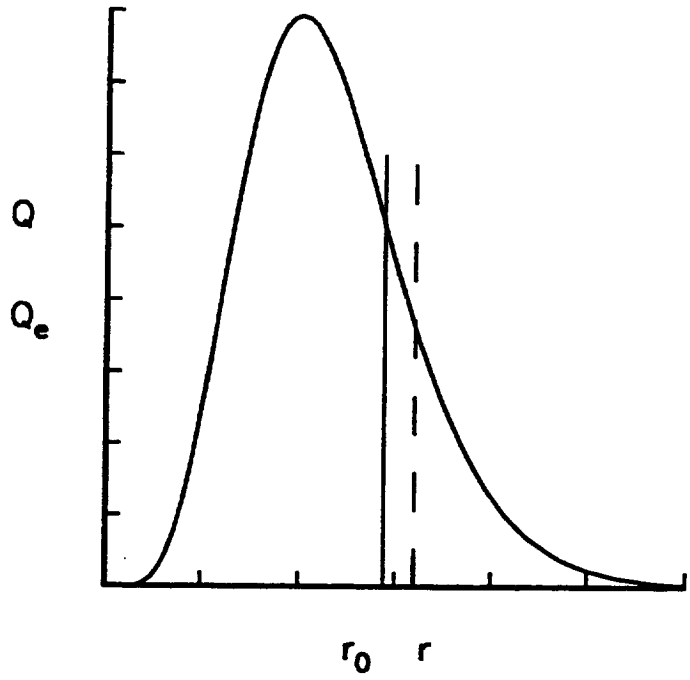

Fig. 2: Graphical solution of eq. (9) (see text).

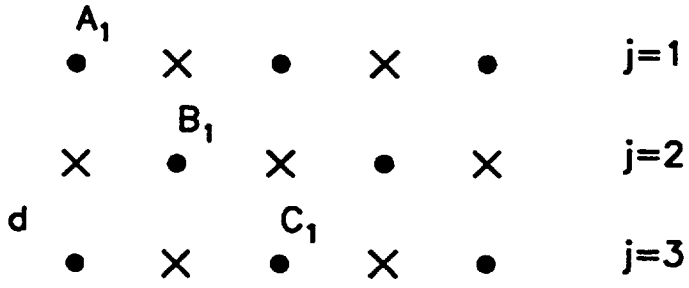

Fig. 3: Side view of a fcc (100) surface. Circles denote atoms on the plane of the page, crosses indicate atoms one plane below or above. The index j labels the planes starting with $j = 1$ for the surface plane.

REPORT DOCUMENTATION PAGE

Form Approved
OMB No. 0704-0188

1. AGENCY USE ONLY (*Leave blank*)	2. REPORT DATE	3. REPORT TYPE AND DATES COVERED
	July 1994	Technical Memorandum

4. TITLE AND SUBTITLE

Modelling of Surfaces

Part I–Monatomic Metallic Surfaces Using Equivalent Crystal Theory

5. FUNDING NUMBERS

WU–505–90–53

6. AUTHOR(S)

Guillermo Bozzolo, John Ferrante, and Agustín M. Rodríguez

7. PERFORMING ORGANIZATION NAME(S) AND ADDRESS(ES)

National Aeronautics and Space Administration
Lewis Research Center
Cleveland, Ohio 44135–3191

8. PERFORMING ORGANIZATION REPORT NUMBER

E–9020

9. SPONSORING/MONITORING AGENCY NAME(S) AND ADDRESS(ES)

National Aeronautics and Space Administration
Washington, D.C. 20546–0001

10. SPONSORING/MONITORING AGENCY REPORT NUMBER

NASA TM–106680

11. SUPPLEMENTARY NOTES

Guillermo Bozzolo, Analex Corporation, 3001 Aerospace Parkway, Brook Park, Ohio 44142–1003 (work funded by NASA Contract NAS3–26776); John Ferrante, NASA Lewis Research Center; and Augustín M. Rodríguez, Departamento de Física, Universidad Nacional de La Plata, C.C. 67, 1900 La Plata, Argentina. Responsible person, John Ferrante, organization code 0130, (216) 433–6069.

12a. DISTRIBUTION/AVAILABILITY STATEMENT

Unclassified - Unlimited
Subject Categories 76 and 26

12b. DISTRIBUTION CODE

13. ABSTRACT ***(Maximum 200 words)***

We present a detailed description of equivalent crystal theory focusing on its application to the study of surface structure. While the emphasis is in the structure of the algorithm and its computational aspects, we also present a comprehensive discussion on the calculation of surface energies of metallic systems with equivalent crystal theory and other approaches. Our results are compared to experiment and other semiempirical as well as first-principles calculations for a variety of fcc and bcc metals.

14. SUBJECT TERMS

Surface structure; Semiempirical methods; Metallic surfaces

15. NUMBER OF PAGES

37

16. PRICE CODE

A03

17. SECURITY CLASSIFICATION OF REPORT	18. SECURITY CLASSIFICATION OF THIS PAGE	19. SECURITY CLASSIFICATION OF ABSTRACT	20. LIMITATION OF ABSTRACT
Unclassified	Unclassified	Unclassified	